Fluid Dynamics & Materials Processing FDMP, vol.16, no.1, pp.121-130, 2020

Aerodynamic Design of a Subsonic Evacuated Tube Train System

Tian Li[1, *], Xiaohan Zhang[1], Yao Jiang[2] and Weihua Zhang[1]

Abstract: The so-called Evacuated Tube Train (ETT) is currently being proposed as a high-speed transportation system potentially competitive with airplane transportation. Aerodynamic resistance is one of the most crucial factors for the successful design of an ETT. In the present work, a three-dimensional concept ETT model has been elaborated. The aerodynamic characteristics of the subsonic ETT have been numerically simulated under different conditions. The train's running speed varies from 600 km/h up to 1200 km/h, and the blockage ratio is in the range between 0.1 and 0.3. As the blocking ratio and running speed increase, the resistance of the head car increases greatly, while the resistance of the middle car changes slightly. The aerodynamic resistance of the tail car is affected by the shock wave emerging in the wake flow. Two different design criteria for the maximum allowed aerodynamic resistance are proposed for aerodynamic parameter matching. With an increase in the blockage ratio and running speed, the atmospheric pressure in the tube should be decreased to achieve a balance.

Keywords: Evacuated tube train, aerodynamic resistance, blockage ratio, shock wave.

1 Introduction

Evacuated tube train (ETT) is a ground-based and high-speed transportation, which can significantly reduce the travel time for a long distance. It can be competitive with the airplane transportation. As the design of the train's running speed is higher than 600 km/h, the aerodynamic characteristics of the train have been attracted majority attentions, especially for the aerodynamic resistance related to the saving energy. For an evacuated tube train, how to design a suitable ETT system with the chosen of several aerodynamic parameters becomes a problem. The aerodynamic parameters include the blockage ratio, the atmosphere in the tube, and so on.

Train shapes affect the aerodynamic resistance of the ETT. Three feasible geometries for the ETT were established [Gillani, Panikulam, Sadasivan et al. (2019)]. The aerodynamic resistance of those simple geometries were calculated under different tube pressures and speeds. The elliptical train shape with a ratio of 2:1 was recommended for the vacuum tube train at 0.1 atm. An aerodynamic design for the Hyperloop vehicle was proposed and initially developed with a 2D Computational Fluid Dynamics (CFD) solver. Three-

[1] State Key Laboratory of Traction Power, Southwest Jiaotong University, Chengdu, 610031, China.

[2] China Railway Eryuan Engineering Group Co., Ltd., Chengdu, 610031, China.

[*] Corresponding Author: Tian Li. Email: litian2008@home.swjtu.edu.cn.

Received: 16 July 2019; Accepted: 14 August 2019.

dimensional simulations were used to evaluate the optimal design. The target aims at either generating a certain lift force or reducing the aerodynamic drag forces [Braun, Sousa and Pekardan (2017)]. Another aerodynamic design of the Hyperloop pod was studied. Its target is to delay the flow separation over the so-called train as much as possible by means of the transition farther upstream, and finally a droplet shape was obtained using the numerical simulation. Meanwhile, the aerodynamic characteristics of the droplet shape were investigated [Opgenoord and Caplan (2018)].

Due to the large resources requirement for the CFD numerical simulations, two-dimensional method has been used to study the aerodynamic characteristics of the ETT. Two-dimensional model of the ETT with pressure recycle ducts was generated and the flow characteristics of those models were numerically simulated in the different supersonic state. The existence of pressure recycle ducts can effectively reduce the aerodynamic pressure by up to 30% [Jia, Wang, Cheng et al. (2018)]. Based an assumption of incompressible flow, the effects of train's running speed, atmosphere in the tube and blockage ratio on the aerodynamic drag of an ETT at subsonic speeds were studied using two-dimensional model in [Zhang (2012)]. The wave phenomena generated by ETT at a super high-speed was studied using two-dimensional axisymmetric method [Zhou, Zhang, Li et al. (2019)]. Results showed that the waves in the tube included expansion waves and shock waves. Several parameters of the ETT system (the atmosphere in the tube, blockage ratio, and running speed) have been investigated using a two-dimensional method in [Kim, Kim and Kwon (2011)]. The guidelines for the initial design on the ETT system were provided.

Up to now, most researches about the aerodynamic characteristics of the ETT are mainly two dimensional. Moreover, the ETT models are simplified greatly. In this paper, a three dimensional ETT model is designed with a considerable streamlined shape. The aerodynamic characteristics of the ETT are numerically simulated using three-dimensional compressible Navier-Stokers equation.

2 Computational information

2.1 Computational model

A concept ETT model is designed as shown in Fig. 1 and used in this investigation. The model consists of a head car, a middle car and a tail car, which are 25.6 m, 25 m and 25.6 m in length, respectively. The length of the whole train is 76.2 m, the train is 3.247 in width and the train height H is 3.64 m. The length of the streamlined nose of the head and tail cars is about 7.5 m. The cross-section area of the train A_{tr} is 10.6 m^2. The gap between the ground and train bottom is 20 mm, which is the levitation height for a super-conductive train. In order to simplify the numerical calculation, the bogies and electrical equipment underneath the train are neglected.

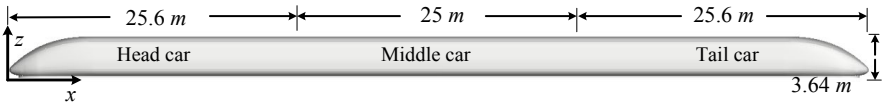

Figure 1: Concept ETT model

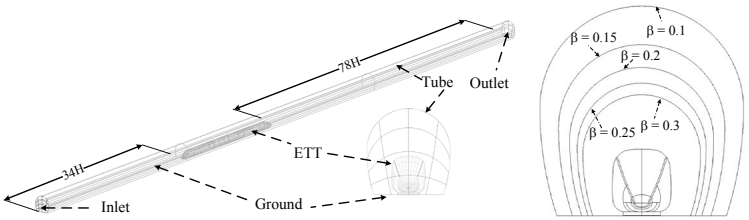

(a) Computational domain (b) blockage ratio

Figure 2: Computational domain and blockage ratio

Fig. 2(a) shows the computational domain. According to the characteristic length H based on the train height, the computational domain is 133 H in length. The entrance is 34 H far from the nose tip of the head car, and the distance between the nose tip of the trail car and the domain exit is 78 H.

Both the entrance and exit of the tube are set as pressure-far-field conditions. The tube, train and ground are set as wall conditions with zero velocity. The air in the tube is considering as an ideal gas and its kinematic viscosity satisfies the Surtherland's law.

Blockage ratio β is one of the most important parameter for the design of ETT system. It is defined as

$$\beta = \frac{A_{\text{tr}}}{A_{\text{tu}}}, \tag{1}$$

where A_{tu} is the cross-section area of the tube.

In this study, 5 different sizes of the blockage ratio are investigated. They are β=0.1, 0.15, 0.2, 0.25 and 0.3.

2.2 Computational mesh

The computational mesh is generated using ANSYS ICEM. It mainly consists of the tetrahedral unstructured grids and boundary layer mesh. Due to the variations of the blockage ratio, the total number of elements is in the range of 20 million and 28 million. Three refinement boxes are added to refine mesh around the train, especially in the wake flow. There are at least 30 layers of mesh in the gap underneath the train. In addition, the non-dimensional size y+ of the train is lower than 2 in most surface due to a small height in the boundary layer. Fig. 3 shows the mesh around the train and the gap.

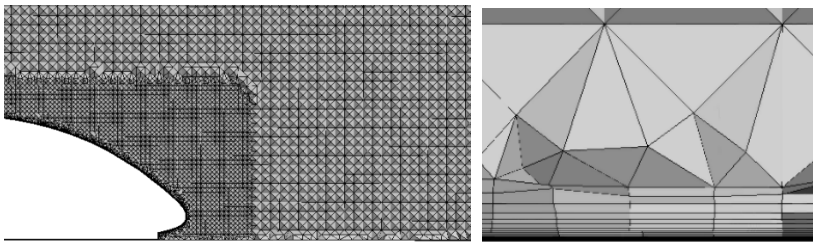

(a) Mesh around the tail car (b) Boundary layer

Figure 3: Computational mesh

2.3 Numerical method

Due to the fact that the Mach number for the considering running speed is higher than 0.3, the air compressibility should be taken into account. Three-dimensional steady compressible Navier-Stokes equations are chosen as the governing equations, and shear stress transport (SST) k-ω turbulence model is adopted. Based on the previous studies [Li, Hemida, Zhang et al. (2018); Li, Qin and Zhang (2019); Li, Zhang, Mohammad et al. (2019)], SST k-ω turbulence model were able to predict accurately the flow around trains.

Density-based solver is chosen for the calculation. The gradient term is discretized using the Green-Gauss Node-Based (GGNB) approach. The second-order upwind scheme is used for both flow and turbulence variant terms. The number of iterations was set as 25000 to achieve a relative stable result.

3 Aerodynamic performances of ETT

Three important aerodynamic parameters for the subsonic ETT are the train's running speed v_{tr}, blockage ratio β and the atmosphere in the tube p_0. In this study, the train's running speed v_{tr} varies from 600 km/h up to 1200 km/h, and 5 different sizes of the blockage ratio β mentioned in Section 2.2 are simulated. Due to the linear relationship between the atmosphere in the tube p_0 and the aerodynamic forces [Liu, Zhang and Zhang (2013)] the effect of the atmosphere in the tube on the aerodynamic forces of the ETT is not studied in the following. The atmosphere at the inlet and outlet boundaries is set as 20265 Pa, which corresponds to be 0.2 atm. The aerodynamic characteristics of the train running in the open air are also studied and compared to those of ETT.

The numerical simulations are performed using the commercial software ANSYS Fluent. In the following, the aerodynamic characteristics of the subsonic ETT are discussed in terms of the aerodynamic resistance of the train under different conditions, the effect of blockage ratio and running speed on the aerodynamic characteristics of trains.

3.1 Aerodynamic resistance of the train under different conditions

Tab. 1 shows the aerodynamic resistance of the train running in the open air or the evacuated tube under the conditions of different blockage ratio size and train's running speed. Compared to the aerodynamic resistance of the train in the open air, the blocking ratio has a drag reduction advantage between 0.1 and 0.15 when the train's running speed is 600 km/h and 700 km/h. When the design speed is 800 km/h and the blocking ratio is lower than 0.15, it can effectively reduce the resistance. When the train's running speed is higher than 900 km/h, there is no drag reduction advantage in almost all kinds of blocking ratios, indicating that it is necessary to reduce the atmosphere inside the tube to achieve a reasonable resistance of the train in the open air. However, when the train's running speed reaches 1200 km/h, the evacuated tube helps reduce the resistance with the blocking ratio less than 0.2. It is mainly related to the shock wave appeared at a different speed around the train. In the open air, the shock wave appears around the train at a Mach number of 1.0, whereas it is advanced in the tube due to the air acceleration.

Table 1: Aerodynamic resistance of the train under different conditions (unit: kN)

		Train speed (km/h)					
		600	700	800	900	1000	1200
Open air		37.22	49.95	66.26	94.83	106.44	242.58
Block ratio	0.1	21.10	30.40	43.49	72.09	117.47	166.35
	0.15	28.64	44.66	62.33	104.42	143.78	196.14
	0.2	39.12	57.89	87.66	129.37	169.88	224.42
	0.25	48.76	72.94	110.16	152.93	193.55	251.34
	0.3	59.27	88.60	129.13	169.61	211.71	274.71

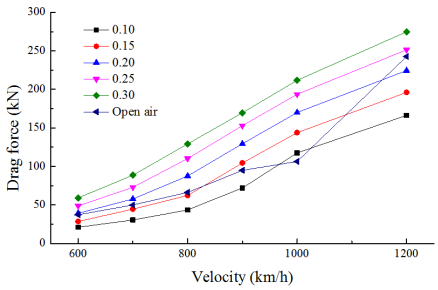

Figure 4: Aerodynamic resistance of the train varied with the blockage ratio and speed

Fig. 4 shows the trends of the aerodynamic resistance varied with the blockage ratio and the train's running speed. The advantage of the blocking ratio and the running speed matching relationship can be seen more intuitively with the help of Fig. 4. It can be seen that the aerodynamic resistance increases with the increase of running speed, and the growth trend of different blocking ratios is the same. For the same running speed, the higher the blocking ratio, the larger the resistance is. The sudden increase in the slope of the resistance is caused by the sudden change in the resistance of the tail car. Those variations are related to the shock wave, which will be analyzed later.

3.3 Effect of blockage ratio on the aerodynamic characteristics

As seen in Fig. 4, when the atmosphere in the tube and the running speed are fixed, the aerodynamic resistance of the ETT gradually increases with the increase of the blocking ratio. Taking the running speed 900 km/h as an example, the aerodynamic resistance composition by each part of the train is analyzed in detail.

Tab. 2 shows the aerodynamic resistance of the train at a speed of 900 km/h varied with the different blocking ratio sizes. It is obvious that as the blocking ratio increases, the resistance of head car becomes larger and larger, the resistance of the middle car change slightly, and that of the tail car also increases with the increase of the blocking ratio. The resistance of

the head and tail cars is mainly made up of the pressure drag force, whereas the viscous drag force contributes the resistance of the middle car. As the blocking ratio increases, the viscous drag force changes slightly and the pressure drag force varies greatly.

Table 2: Aerodynamic resistance of the train at a speed of 900 km/h (unit: kN)

	Blockage ratio β				
	0.10	0.15	0.20	0.25	0.30
Head car	30.34	41.22	52.37	64.78	75.50
Middle car	4.30	4.56	4.64	5.28	5.51
Tail car	37.45	58.63	72.36	82.88	88.60
Whole train	72.09	104.42	129.37	152.93	169.61

As shown in Fig. 5, the pressure distribution around the head car varied with different blocking ratio at a speed of 900 km/h is extracted. It can be seen that the maximum pressure appear at the nose tip. When the blocking ratio is 0.1, the high pressure zone near the nose tip of the train is between 11,000 Pa and 14000 Pa. When the blocking ratio increases to 0.15, the high pressure region becomes large, resulting in a larger head resistance. Similarly, when the blocking ratio is up to 0.3, the high pressure zone close to the nose tip of the train can reach about 17,000 Pa. Therefore, the aerodynamic resistance of the head car increases as the blocking ratio increases.

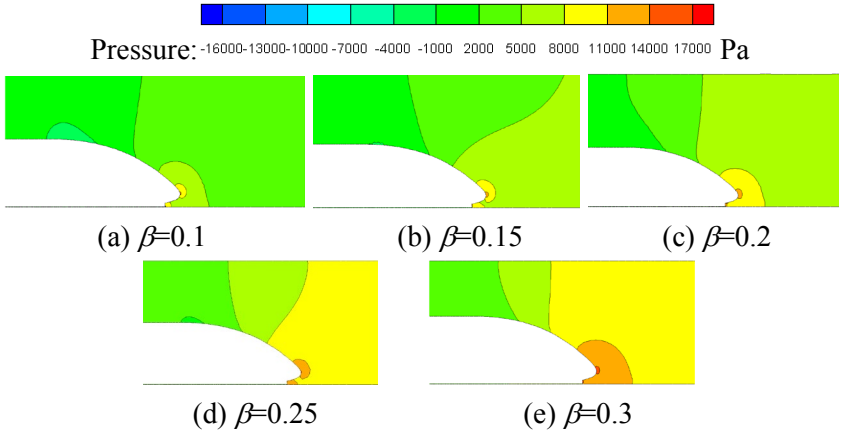

Figure 5: Pressure distribution around the head car varied with the blockage ratio at a speed of 900 km/h

As discussed above, the resistance of the middle car changes slightly, therefore, the flow field around the middle car will not be discussed any more. Figs. 6 and 7 show the velocity and pressure distributions around the tail car varied with the blockage ratio at a speed of 900 km/h, respectively. When the blocking ratio is 0.1, the flow velocity around the tail car can reach as high as 300 m/s, resulting in a partial low pressure region as shown in Fig. 7(a). As the blocking ratio increases, the gap between the tube and train

becomes smaller. When the air flow over the roof of the tail car, the flow velocity increases and a low-pressure region is formed. It is attached to the tail car, which makes an increase in the pressure drag force of the tail car. The accelerating air flow compresses with a slower velocity and thus a shock wave is generated. When the blocking ratio becomes larger, the generated shock wave is reflected in the tube at the rare of the tail car. Meanwhile, the area of the low pressure region attached to the tail car become larger, consequently, the aerodynamic resistance of the tail car increases, as shown in Fig. 7(c).

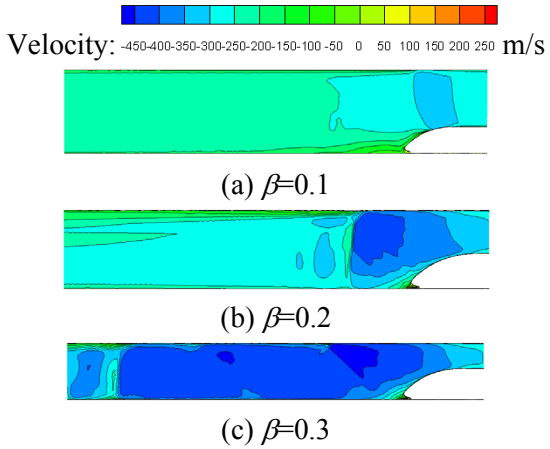

(a) β=0.1

(b) β=0.2

(c) β=0.3

Figure 6: Velocity distribution around the tail car varied with the blockage ratio at a speed of 900 km/h

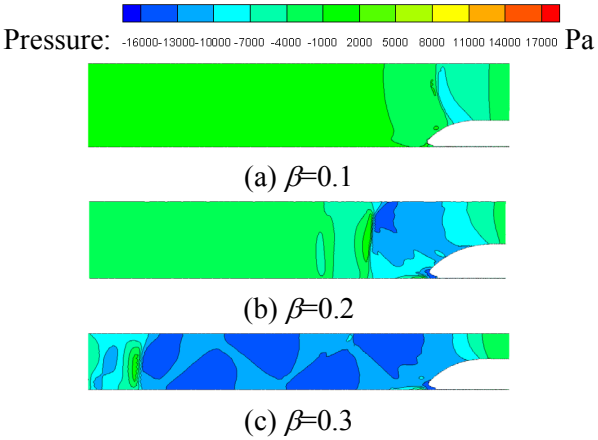

(a) β=0.1

(b) β=0.2

(c) β=0.3

Figure 7: Pressure distribution around the tail car varied with the blockage ratio at a speed of 900 km/h

3.4 Effect of running speed on the aerodynamic characteristics

According to Section 3.1, we know that the aerodynamic resistance of the train increases with the increase of the train's running speed, and the variations for each blocking ratio is basically the same. Hereby, taking the blocking ratio of 0.25 as an example, the aerodynamic drag changes of the individual car are specifically analyzed.

Table 3: Aerodynamic resistance of the train at a blocking ratio of 0.25 (unit: kN)

	Train speed (km/h)					
	600	700	800	900	1000	1200
Head car	26.40	37.25	50.06	64.78	81.64	131.56
Middle car	1.54	2.95	3.57	5.28	6.22	9.69
Tail car	20.82	32.74	56.54	82.88	105.69	110.09
Whole train	48.76	72.94	110.16	152.93	193.55	251.34

Tab. 3 shows the aerodynamic resistance of the train with different running speed at a blocking ratio of 0.2. As the train's running speed increases, the resistance of the head car increases greatly and that of the middle car change slightly. The resistance of the tail car increases greatly when its speed lower than 900 km/h, and then it increases slowly in the range of 1000 km/h and 1200 km/h.

In order to study the aerodynamic resistance of the tail car, the pressure distribution around the tail car is given Fig. 8. As the running speed increases, the airflow above the roof of the tail car will flow faster. When the speed reaches 700 km/h, the slight shock wave is initially formed around the tail car, which is attached to the low pressure area close to the tail car. When the speed is up to 900 km/h, the region with a pressure between -1,000 Pa to -12,000 Pa is attached to the tail nose, therefore, the pressure drag force is the maximum. When the speed exceeds 900 km/h, the shock wave will slowly reflect in the wake behind the tail car, and the pressure amplitude in the low pressure region becomes smaller. When the speed is 1200 km/h, the low pressure attached to the tail car ranges from -8000 Pa to -1000 Pa, which makes the resistance of the tail train increasing slightly.

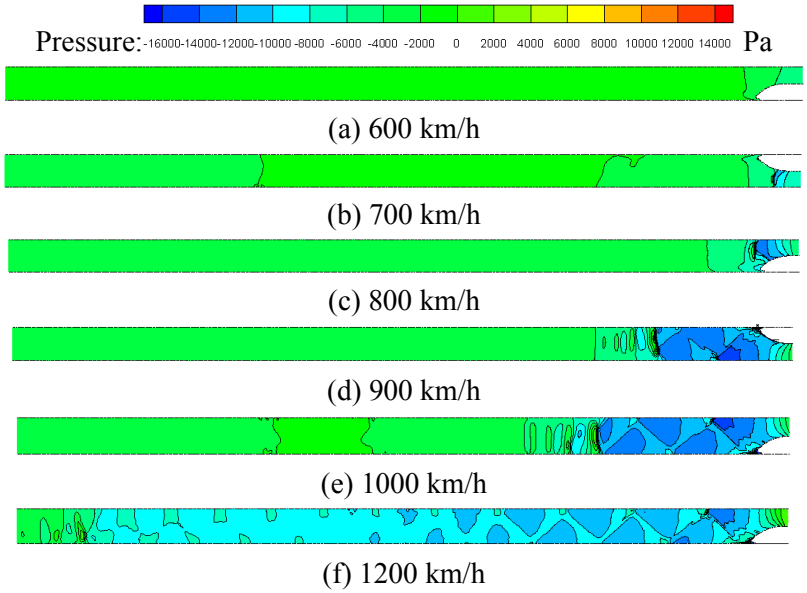

Figure 8: Pressure distribution around the tail car at a blockage ratio of 0.2

4 Aerodynamic parameter design

The aerodynamic parameter matching is the paramount factor for the ETT design. In this section, two design criteria for the maximum allowed aerodynamic resistance are proposed. One is the aerodynamic resistance of the train running in the open air with a speed of 600 km/h, which is F_{ref}=37.22 kN, and the other one is F_{ref}=50 kN based on the assumption that the design power for the ETT can overcome the maximum aerodynamic resistance.

Fig. 9 shows the matching aerodynamic parameters for the subsonic ETT based on the above criteria. With the increase of the blockage ratio, the atmosphere in the tube should be decreased to achieve a balance for the aerodynamic resistance. Meanwhile, the atmosphere in the tube should be designed to be lower when the design of the running speed is higher.

For the first criterion, when the design speed is 600 km/h, the atmosphere in the tube 0.35 atm is recommend for the blockage ratio of 0.1, and 0.13 atm is suggested for the blockage ratio of 0.3. For the second criterion, when the design speed is 600 km/h, the atmosphere in the tube 0.47 atm is recommend for the blockage ratio of 0.1, and 0.16 atm is suggested for the blockage ratio of 0.3. Due to the linear relationship, the ratio between the atmosphere in the tube for the second and first criterion is almost same as the ratio between the reference aerodynamic resistances.

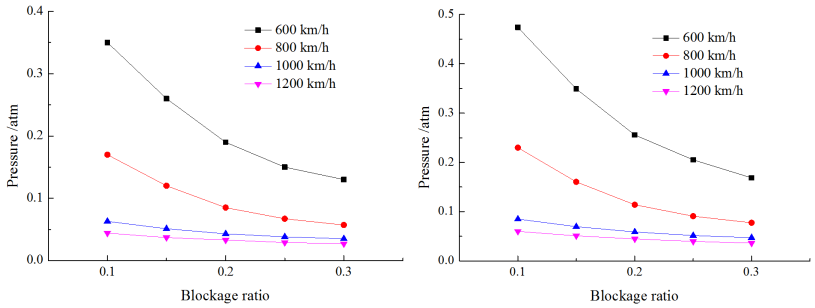

(a) F_{ref}=37.22 kN (b) F_{ref}=50 kN

Figure 9: Aerodynamic parameter design based on different reference resistances

5 Conclusion and discussion

(1) The effect of the blockage ratio on the aerodynamic characteristics of the ETT is studied. As the blocking ratio increases, the resistance of head car becomes larger and larger, the resistance of the middle car change slightly, and that of the tail car also increases with the increase of the blocking ratio.

(2) The effect of the running speed on the aerodynamic characteristics of the ETT is studied. As the train's running speed increases, the resistance of the head car increases greatly and that of the middle car change slightly. The resistance of the tail car increases greatly when its speed lower than 900 km/h, and then it increases slowly in the range between 1000 km/h and 1200 km/h.

(3) Two design criteria for the maximum allowed aerodynamic resistance are proposed. With the increase of the blockage ratio, the atmospheric pressure in the tube should be decreased to achieve a balance for the ideal aerodynamic resistance. Meanwhile, the

atmospheric pressure in the tube should be designed to be lower when the design of the running speed is higher.

(4) There are other ways to reduce the aerodynamic resistance of the ETT, such as decreasing the cross-section area of the train, a longer streamlined nose of the train, some effective tools to eliminate or delay the shock waves emerging in the wake flow.

Acknowledgement: This work was supported by Sichuan Science and Technology Program (No. 2019YJ0227), China Postdoctoral Science Foundation (No. 2019M663550), China Postdoctoral Science Foundation (No. 2019M663550) and Science and Technology Program of China Railway Group Limited (No. 2018-S-02).

Conflicts of Interest: The authors declare that they have no conflicts of interest to report regarding the present study.

References

Braun, J.; Sousa, J.; Pekardan, C. (2017): Aerodynamic design and analysis of the hyperloop. *AIAA Journal*, vol. 55, no. 12, pp. 4053-4060.

Jia, W.; Wang, K.; Cheng, A.; Kong, X.; Cao, X. et al. (2018): Airflow and differential pressure characteristics in the vacuum tube transportation system based on pressure recycle ducts. *Vacuum*, vol. 150, no. 2018, pp. 58-68.

Kim, T.; Kim, K.; Kwon, H. (2011): Aerodynamic characteristics of a tube train. *Journal of Wind Engineering & Industrial Aerodynamics*, vol. 99, no. 12, pp. 1187-1196.

Li, T.; Hemida, H.; Zhang, J.; Mohammad, R.; Flynn, D. (2018): Comparisons of shear stress transport and detached eddy simulations of the flow around trains. *Journal of Fluids Engineering*, vol. 140, no. 11, pp. 111108-111112.

Li, T.; Qin, D.; Zhang, J. (2019): Effect of RANS turbulence model on aerodynamic behavior of trains in crosswind, *Chinese Journal of Mechanical Engineering*, vol. 32, pp. 1-12.

Liu, J.; Zhang, J.; Zhang, W. (2013): Analysis of aerodynamic characteristics of high-speed trains in the evacuated tube. *Journal of Mechanical Engineering*, vol. 49, no. 22, pp. 137-143 (In Chinese).

Opgenoord, M. M. J.; Caplan, P. C. (2018): Aerodynamic design of the hyperloop concept. *AIAA Journal*, vol. 56, no. 11, pp. 4261-4270.

Zhang, Y. P. (2012): Numerical simulation and analysis of aerodynamic drag on a subsonic train in evacuated tube transportation. *Journal of Modern Transportation*, vol. 20, no. 1, pp. 44-48.

Zhou, P.; Zhang, J.; Li, T.; Zhang, W. (2019): Numerical study on wave phenomena produced by the super high-speed evacuated tube maglev train. *Journal of Wind Engineering & Industrial Aerodynamics*, vol. 190, pp. 161-70.

Gillani, S. A.; Panikulam, V. P.; Sadasivan, S.; Zhang. Y. P. (2019): CFD analysis of aerodynamic drag effects on vacuum tube trains. *Journal of Applied Fluid Mechanics*, vol. 12, no. 1, pp. 303-309.